sustainability

MDPI

Article

Nutritional Quality of the "Algarrobo" *Neltuma pallida* Fruit and Its Relationship with Soil Properties and Vegetation Indices in the Dry Forests of Northern Peru

Wilian Salazar [1,*], Camila Cruz-Grimaldo [1], Sphyros Lastra [2], Raihil Rengifo [3], Celia Vargas-de-la-Cruz [4], David Godoy-Padilla [3], Emmanuel Sessarego [3], Juancarlos Cruz [3] and Richard Solórzano [3,5]

[1] Estación Experimental Agraria Vista Florida, Instituto Nacional de Innovación Agraria (INIA), Lima 15024, Peru; camila.cruz239@gmail.com
[2] Dirección de Recursos Genéticos Vegetales, Instituto Nacional de Innovación Agraria (INIA), Lima 15024, Peru; slastra@inia.gob.pe
[3] Dirección de Supervisión y Monitoreo en las Estaciones Experimentales Agrarias, Instituto Nacional de Innovación Agraria (INIA), Lima 15024, Peru; raihil2209@gmail.com (R.R.); davgodoy1@gmail.com (D.G.-P.); investigacion_procap@inia.gob.pe (E.S.); jcruz@inia.gob.pe (J.C.); investigacion_labsaf@inia.gob.pe (R.S.)
[4] Department of Pharmacology, Bromatology and Toxicology, Faculty of Pharmacy and Biochemistry, Universidad Nacional Mayor de San Marcos, Lima 15001, Peru; cvargasd@unmsm.edu.pe
[5] Facultad de Ciencias Ambientales, Universidad Científica del Sur (UCSUR), Lima 15067, Peru
* Correspondence: wilian-salazar@hotmail.es

Abstract

The dry forests of northern Peru are home to extensive populations of algarrobo (*Neltuma* spp.). Its fruit serves as feed for goats and is used in various agro-industrial products. However, the nutritional quality can be influenced by the physicochemical properties of the soil and vegetation coverage. The objective of this study was to understand and predict the concentration of protein and ether extracts of carob and evaluate its relationship with soil properties and vegetation indices. Principal component analysis (PCA) and correlation analyses were conducted. The prediction of protein and ether extract was carried out using the Eureqa-Formulize software 1.24.0. In the PCA, protein showed a positive relationship with ash and ether extract but a negative relationship with moisture. Likewise, moderate correlations were observed between protein and ash content (0.51). Protein also showed positive correlations with pH (r = 0.19), BI (r = 0.22), and NDSI (r = 0.22). Additionally, the ether extract exhibited correlations with sand content (r = 0.22), Ca^{2+} (r = −0.26), Cu (r = −0.20), S5 (r = 0.26), and Si (r = 0.24). Protein predictions showed moderate performance (CC = 0.73 and R^2 = 0.53), as did ether extracts (CC = 0.68 and R^2 = 0.46). These findings contribute to a better understanding of the factors that influence the nutritional quality of carob and can be used for the development of sustainable management strategies in the dry forests of northern Peru.

Keywords: carob pobs; ether extract content; forecasting equations; protein content; vegetation indices; soil

Academic Editor: Anna De Marco

Received: 28 April 2025
Revised: 5 June 2025
Accepted: 20 June 2025
Published: 16 September 2025

Citation: Salazar, W.; Cruz-Grimaldo, C.; Lastra, S.; Rengifo, R.; Vargas-de-la-Cruz, C.; Godoy-Padilla, D.; Sessarego, E.; Cruz, J.; Solórzano, R. Nutritional Quality of the "Algarrobo" *Neltuma pallida* Fruit and Its Relationship with Soil Properties and Vegetation Indices in the Dry Forests of Northern Peru. *Sustainability* **2025**, *17*, 8296. https://doi.org/10.3390/su17188296

1. Introduction

The tropical dry forest represents 50% of the forested areas in Central America and 22% in South America [1]. In Peru, individuals of the genus *Neltuma*, known as carob trees, are found in the dry forests of La Libertad, Lambayeque, Piura, and Tumbes [2,3] and play a fundamental role in the ecological balance of this biome [4]. Carob trees contribute to

the control of water erosion, improve soil fertility, favor the survival of local fauna, and regulate the climate [5]. They also play key roles in soil bioremediation and constitute a valuable timber and fodder resource for local communities [5,6].

Carob fruits, known as "algarroba", are an essential food resource for humans and animals in arid and semi-arid regions [7]. In 2023 and 2024 in Peru, the estimated production of algarroba reached 445 and 341 tons, respectively [8]. The algarroba is essential for feeding cattle and goats in the dry forest [9], particularly during prolonged periods of drought. Due to its importance in the local diet and economy, optimizing carob production and improving its nutritional quality is crucial to meet the growing demand of an expanding population [10,11]. However, studies evaluating the relationship between soil composition and the nutritional quality of carob are limited, leaving a knowledge gap on how edaphic conditions can influence the concentration of the proteins and fats of this fruit. Soil properties have been shown to significantly affect the quality of various crops, such as blueberries, tomatoes, cotton, sugarcane, and citrus, through their impact on nutrient uptake and storage of biochemical compounds in fruits [12–17].

The analysis of soil properties and environmental variables has an important impact on fruit quality, but there are limitations due to the high costs of the analyses and the difficulty of covering large areas of land [18]. In this context, new techniques such as remote sensing and vegetative index analysis have emerged as efficient alternatives to assess and manage soil quality as well as its impact on crops [19,20]. Although remote sensing methods have certain limitations, such as capturing soil heterogeneity and depth, as well as spatial spectral resolution, in addition to calibration and validation requirements [21,22], their advantages make them indispensable tools for agriculture and crop management.

Protein estimation by remote sensing is essential for managing crop nutritional quality [23]. Satellite imagery has been used to predict protein concentrations in rice and wheat crops [24,25]. Like the previous applications, satellite images have also been used to estimate soil parameters such as salinity, organic carbon, and pH, using vegetation indices [21,26]. It is established that the variation in reflectance between the visible, near infrared (NIR), and shortwave infrared (SWIR) bands is most used to determine specific soil characteristics, such as salinity. In the case of carob, remote sensing studies have been developed to analyze the change in land use coverage, using vegetation indices [27], as well as to model the current and future potential distribution of the *Neltuma* habitat [28].

Despite the importance of carob in dry forest ecosystems, few studies integrate the analysis of the nutritional quality of the fruit with soil characterization and vegetation indices. In this context, the present study aims to evaluate the influence of soil physicochemical properties on the composition and nutritional quality of carob, through chemical analysis and data obtained from satellite images, with which we seek to predict the content of protein and ether extract. The results are expected to provide key information for designing sustainable management strategies for carob, promoting the preservation of the dry forest, enhancing ecosystem services, and improving the well-being of local communities that depend on this resource.

2. Materials and Methods

2.1. Study Area

The study was conducted in five provinces of the Piura region, Talara, Sullana, Piura, Morropón, and Sechura, in February and March 2024, located at the following geographic coordinates: −4.956° latitude, −80.53° longitude. In the productive areas surrounding the forests, crops such as rice, corn, bananas, and fruit trees like mangoes are grown. This area is characterized by a mean annual precipitation of 49 mm and a maximum daily temperature of 34.5 °C, recorded in March [9]. Like other regions on the northern coast of Peru, Piura is

also affected by the El Niño-Southern Oscillation (ENSO), with an accumulated rainfall of 2500 mm [29]. This precipitation refills the aquifers and is vital for the development of dry forest and carob trees. The selection of sampling points (SPs) focused on areas with carob presence and goat grazing activities. These areas were identified based on the studies of [30] for the distribution of carob and [31] for the location of localities with a high presence of goats. Once the goat paddocks were located, a 4 km buffer was generated around them, which was intersected with the distribution of carob trees. In the areas resulting from the intersection, random SP were established using the QGIS 3.34.7 tool "Determination of random points". Although these points served as an initial reference for sampling, several of them proved to be inaccessible, so it was decided to sample trees near the access roads. The selected trees had to be in the fruiting phase, with pods in the ripening stage, to guarantee fruit collection. A total of 71 SP were evaluated; soil and fruit samples were collected from each of them. The distribution of the SP is shown in Figure 1.

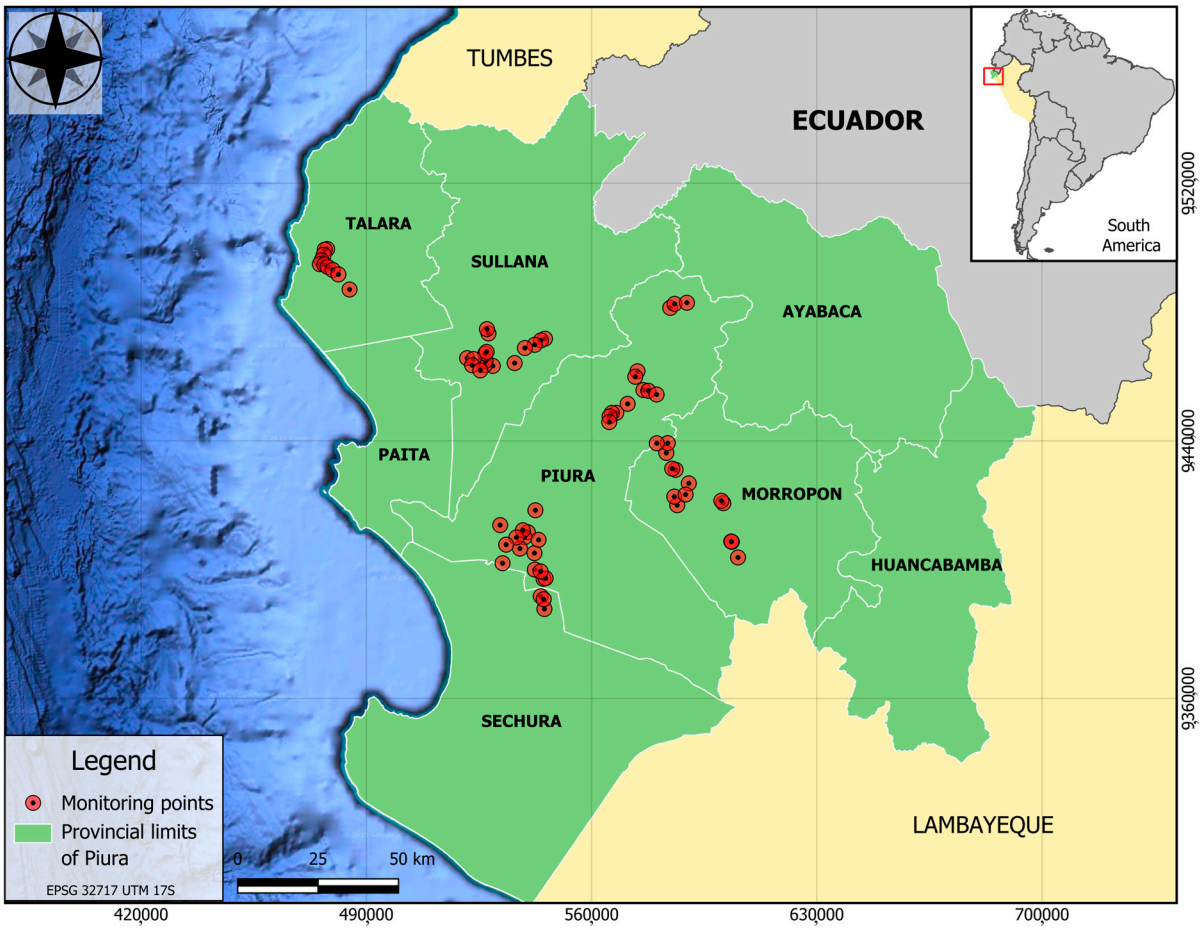

Figure 1. Locations for sampling points in the five provinces of the Piura region, Peru.

2.2. Analysis and Sampling

2.2.1. Soil Sampling

Soil samples were collected at a depth of 30 cm and were located at the outer limit of the canopy projection on the soil. The distance between the trunk and the subsample sampling sites varied according to the tree's canopy size, ranging from 8 to 12 m. For each tree, four subsamples were taken at the four cardinal points (north, south, east, and west), which were homogenized to form a composite sample representative of the zone with root influence. The samples were stored in airtight polyethylene bags to prevent contamination and moisture loss and were transported under controlled conditions to the Soil, Water, and

Fertilizer Laboratory (LABSAF) of the National Institute for Agrarian Innovation (INIA), Peru, for analysis. The physicochemical parameters evaluated are detailed in Table 1.

Table 1. Soil physicochemical properties and methods used in the laboratory.

Parameters Assessed	Method and/or Instrument	Remark	Source
pH	Digital potentiometer	soil suspension: water (1:2.5)	[32]
Electrical conductivity (EC)	Digital conductivity meter	Same suspension of pH analysis	[33]
Organic matter (OM)	Walkley-Black wet oxidation		[34]
Texture	Bouyucos method		[35]
Cation-exchange capacity (CEC)	Ammonium acetate	pH 7	[35]
Nutrients available	Flamometry: exchangeable potassium		[35]
	Bray II: phosphorus available		[35]
	Kjeldahl: total nitrogen		[36]
Heavy metals	Inductively coupled plasma mass spectrometry		[37]

2.2.2. Evaluation of the Carob Nutritional Quality

Mature plant material was collected from the same trees from which the soil samples were taken. Carob pods were placed in paper bags until a minimum weight of 100 g was reached, then transferred to the laboratory for drying. The samples were then taken to the Food Analysis Laboratory of the Nutritional Research Institute, where they underwent grinding and chemical analysis to determine ether extract and protein concentrations. In addition, moisture and ash parameters were evaluated. Moisture was determined according to NTP 208.017:2021: cocoa and chocolate using the gravimetric method [38]. For the esther extract, NTP 208.016:2021: cocoa and chocolate used the Soxhlet extraction method [39]. Crude protein was determined according to AOAC 2001.11 Edition 2023: Protein Crude assay in Animal Feed, Forage (Plant Tissue), Grain, and Oil Seeds. Block Digestion Method Using Copper Catalyst and Steam Distillation into Boric Acid [40]. For ash AOAC 930.05, Ash of plants [41].

2.3. Multispectral Data Collection and Processing

The vegetation indices (VIs) were calculated from Landsat-8 sensor satellite images, using the Python programming language (version 3.8, Python Software Foundation) in the Jupyter Lab environment, with the Google Earth Engine extension [42]. The relation of VIs is detailed in Table 2. For their compilation, the Python libraries Geemap [43], os, and Geopandas [44] were also used. To generate the orthomosaic covering the entire study area, images acquired on three different dates were merged: March 6, April 7, and May 2. These dates were chosen due to their low cloud cover ($\leq$20%), as in previous periods the cloud cover in the area was high (>20%), which affected the quality of the data. Once the VIs were obtained, the values were extracted within a 90 m radius influence area, using the sampling point (SP) as the centroid. This strategy minimized the influence of outliers associated with the spectral variability in a single pixel. Finally, the values obtained were matched to the protein and ether extract concentration in the carob and used for building the predictive models.

Table 2. Vegetation indices calculated from Lansat-8 satellite images.

Vegetation Index	Equation	Source
Brightness Index (BI)	$\left(\frac{Red^2+Green^2+Blue^2}{3}\right)^{0.5}$	[45]
Coloration Index (COI)	$\frac{Red-Green}{Red+Green}$	[46]
Difference Vegetation Index (DVI)	$NIR - Red$	[47]
Enhanced Vegetation Index (EVI)	$\frac{NIR-Red}{(NIR+Red+0.5)\times(1+0.5)}$	[48]
Greenness Index (GI)	$\frac{2Green-Red-Blue}{2Green+Red+Blue}$	[49]
Grain Size Index (GSI)	$\frac{Red-Blue}{Red+Blue+Green}$	[50]
Global Vegetation Index (GVI)	$(-0.29 \times \text{Green}) - (0.56 \times \text{Red}) + (0.6 \times \text{IR}) + (0.49 \times \text{NIR})$	[51]
Infrared Percentage Vegetation Index (IPVI)	$\frac{NIR}{(NIR+Red)}$	[52]
Normalized Burn Ratio (NBR)	$\frac{NIR-SWIR2}{NIR+SWIR2}$	[53]
Normalized Difference Salinity Index (NDSI)	$\frac{Red-NIR}{Red+NIR}$	[54]
Normalized Difference Vegetation Index (NDVI)	$\frac{NIR-Red}{NIR+Red}$	[55]
Normalized Difference Water Index (NDWI)	$\frac{Green-NIR}{Green+NIR}$	[56]
Salinity Index (S1)	$\frac{Blue}{Red}$	[57]
Saturation Index (SI)	$\frac{Red-Blue}{Red+Blue}$	
Redness index (RI)	$\frac{Red^2}{Blue\times Green^3}$	[46]
Salinity Index (S2)	$\frac{Blue-Red}{Blue+Red}$	
Salinity Index (S3)	$\frac{Green\times Red}{Blue}$	[58]
Salinity Index (S4)	$\frac{Blue\times Red}{Green}$	
Salinity Index (S5)	$\frac{Red\times NIR}{Green}$	[45]
Salinity Index (S6)	$(Blue \times Red)^{0.5}$	
Salinity Index (S7)	$(Green \times Red)^{0.5}$	[59]
Soil Adjusted Vegetation Index (SAVI)	$\frac{(NIR-Red)(1+L)}{(NIR+Red+L)}$	[60]
Saturation Index (SI)	$\frac{Red-Blue}{Red+Blue}$	[46]
Transformed Soil Adjusted Vegetation Index (TSAVI)	$\frac{a(NIR-aRed-b)}{Red+a(NIR-b)+x(1+a^2)}$ Donde a = 0.33, b = 0.5, x = 1.5	[61]
Wetness Index (WI)	$\frac{NIR-SWIR1}{NIR+SWIR1}$	[56]
Redness index (RI)	$\frac{Red^2}{Blue\times Green^3}$	[46]
Ratio Vegetation Index (RVI)	$\frac{NIR}{RED}$	[62]
Ferric Iron Index (FI)	$\frac{Red}{Blue}$	[63]
Clay Index (CI)	$\frac{SWIR1}{SWIR2}$	[64]

2.4. Generation of Protein and Ether Extract Prediction Equations

The generation of equations to estimate the protein and ether extract content of carob pods was carried out using the Eureqa-Formulize software 1.24.0 (Noutonian, Newton, MA, USA). This software allows the generation of equations and hidden mathematical relationships [65]. The input variables were the soil properties and VI detailed in Table 2, with protein and ether extract concentrations as output variables. In the preprocessing of the input data before starting the generation of the equations, the outlier removal and the variable normalization of those that did not match normality were carried out. For each of the predicted variables, multiple equations were generated in order to select the one

with the best performance. The selection of the model was based on those that presented the highest values of determination coefficient (R^2) and those that showed the best results according to other indicators of fit quality [66].

2.5. Statistical Analysis

Data were analyzed using R software (version 4.2). Statistical analyses were performed to evaluate differences in soil physicochemical properties, carob nutritional quality, and VI. Pearson correlation analyses were also performed to analyze the relationship between variables, as well as the use of principal component analysis (PCA). In the case of Pearson, the Bonferroni correction was used. The performance of the generated equations was evaluated by comparing the simulated values with the observed values using the following indicators: coefficient of determination (R^2), mean absolute error (MAE), mean square error (MSE), and correlation coefficient (CC). The equations were chosen on the basis of their indicators' performance. The equations used are as follows: 1, 2, 3, and 4.

$$R^2 = \frac{\sum_{i=1}^{n}(T_i - \overline{T})\ (t_i - \overline{t})}{\sqrt{\sum_{i=1}^{n}(T_i - \overline{T})^2 \sum_{i=1}^{n}(t_i - \overline{t})^2}} \quad (1)$$

$$MAE = \frac{1}{n}\sum_{i=1}^{n}|T_i - t_i| \quad (2)$$

$$MSE = \frac{1}{n}\sum_{i=1}^{n}(T_i - t_i)^2 \quad (3)$$

$$CC = \sqrt{R^2} \quad (4)$$

where n is the number, T_i is the original measured values, t_i is the predicted values in the stablished model, and bar shows the average value of the variable referred to.

3. Results

3.1. Analysis of Soil Physicochemical Properties, Fruit Quality, and Vegetation Indices

3.1.1. Soil Physicochemical Properties

Table 3 presents the average values of the soil physicochemical properties at the evaluated points. The electrical conductivity (EC) showed an average value of 85.93 mS cm^{-1}, with a range between 3.71 and 966.40 mS cm^{-1}, indicating variability in soil salinity. The pH ranged from 4.40 to 8.10, with a mean value of 7.00, reflecting acidic to slightly alkaline conditions. The organic matter (OM) content ranged from 0.86% to 12.99%, with an average of 4.65%, while total nitrogen (TN) presented low values, with an average of 0.01%. As for available nutrients, potassium (K_{avai}) and phosphorus (P*avai*) presented average values of 130.08 ppm and 6.91 ppm, respectively, with a high variability in their concentration. The soil texture was mainly composed of a sand fraction, with an average content of 84.68%, while clay and silt showed average values of 8.60% and 6.72%, respectively. Regarding the cation exchange capacity, calcium (Ca^{2+}) was the predominant cation, with a mean of 4.36 $cmol^+/kg$, followed by magnesium (Mg^{2+}) (0.81 $cmol^+\ kg^{-1}$), sodium (Na^+) (0.50 $cmol^+\ kg^{-1}$), and exchangeable potassium (K^+) (0.37 $cmol^+\ kg^{-1}$). Finally, the total carbon (TC) and organic carbon (OC) contents showed mean values of 3.72% and 2.66%, respectively, with moderate variability.

Table 3. Statistical analysis of the soil physicochemical properties.

Properties	Units	Mean	Maximum	Minimum	Standard Deviation (±)
Electrical conductivity (EC)	mS cm^{-1}	85.93	966.40	3.71	184.81
pH	-	7.00	8.10	4.40	0.56
Potassium available (K_{avai})	ppm	130.08	600.42	40.31	110.35
Phosphorus available (P_{avai})		6.91	48.70	0.00	8.00
Organic matter (OM)		4.65	12.99	0.86	2.38
Total nitrogen (TN)		0.01	0.03	0.00	0.01
Sand	%	84.68	98.44	38.29	7.31
Clay		8.60	17.56	1.14	3.75
Silt		6.72	44.14	0.28	5.36
Total carbon (TC)		3.72	9.30	0.81	1.46
Carbon organic (OC)		2.66	7.53	0.50	1.44
Calcium ion (Ca^{2+})	cmol^{+} kg^{-1}	4.36	28.47	0.88	5.49
Magnesium ion (Mg^{2+})		0.81	5.33	0.00	0.99
Sodium ion (Na^{+})		0.50	8.02	0.00	1.56
Potassium ion (K^{+})		0.37	3.10	0.10	0.43

3.1.2. Presence of Metals in Soil

The metals present in the soil (Table 4) show that iron (Fe), calcium (Ca), and aluminum (Al) were the most abundant elements, with averages of 9046.52 ppm, 5532.15, and 6716.76 ppm, respectively. Additionally, there was a significant dispersion in their values, as reflected in the high standard deviation values. In contrast, mercury (Hg) and thallium (Tl) presented low concentrations, with averages of 0.05 and 0.16 ppm, respectively, and lower variability. Arsenic (As) had a mean of 41.59 ppm and a standard deviation of 7.66 ppm, showing moderate dispersion, while cobalt (Co), copper (Cu), and zinc (Zn) had mean values of 6.14, 16.46, and 65.63 ppm, respectively. Manganese (Mn) and potassium (K) with averages of 3130.53 and 1591.56 ppm, respectively, showed high variability, as indicated by the standard deviations of 172.81 and 770.42 ppm, respectively. Other metals include beryllium (Be), cadmium (Cd), lead (Pb), selenium (Se), nickel (Ni), strontium (Sr), and vanadium (V). The average values found in this study are Sr = 78.42 > V = 65.29 > Ni = 9.64 > Pb = 9.12 > Se = 4.64 > Cd = 0.92 > Be = 0.38 ppm. Molybdenum (Mo), sodium (Na), barium (Ba), antimony (Sb), manganese (Mn), and chlorine had average concentrations of 0.76, 700.93, 60.65, 0.31, 275.88, and 19.06 ppm, respectively, with mixed standard deviations.

Table 4. Statistical analysis of metals present in the soil.

Properties (ppm)	Mean	Maximum	Minimum	Standard Deviation (±)
Arsenic (As)	41.59	59.65	29.23	7.66
Beryllium (Be)	0.38	1.00	0.00	0.19
Cadmium (Cd)	0.92	2.70	0.30	0.56
Calcium (Ca)	5532.15	20,615.35	2876.40	3056.64
Cobalt (Co)	6.14	20.20	1.89	4.32
Copper (Cu)	16.46	58.05	4.23	11.96
Strontium (Sr)	78.42	213.99	36.88	35.89
Molybdenum (Mo)	0.76	1.88	0.32	0.37
Nickel (Ni)	9.64	37.17	3.26	7.29
Lead (Pb)	9.12	33.18	3.05	5.19
Selenium (Se)	4.64	14.07	0.00	2.77
Thallium (Tl)	0.16	0.48	0.04	0.11
Vanadium (V)	65.29	139.90	43.32	22.04

Table 4. *Cont.*

Properties (ppm)	Mean	Maximum	Minimum	Standard Deviation (±)
Iron (Fe)	9046.52	22,008.29	4050.02	4644.70
Potassium (K)	1591.56	4667.54	498.19	770.42
Magnesium (Mg)	3130.53	8352.83	1023.90	1536.74
Sodium (Na)	700.93	6819.66	78.93	1324.26
Mercury (Hg)	0.05	0.82	0.00	0.15
Barium (Ba)	60.65	275.93	10.28	52.87
Zinc (Zn)	65.63	144.00	29.65	29.30
Antimony (Sb)	0.31	0.57	0.18	0.08
Manganese (Mn)	275.88	913.85	98.08	172.81
Chromium (Cr)	19.06	41.13	11.38	6.67
Aluminum (Al)	6716.76	14,559.98	2961.31	2948.43

3.1.3. Nutritional Quality of Carob

The humidity content (Table 5) presented an average of 12.11%, with a standard deviation of ±0.74 g 100 g^{-1}, which indicates a moderate variability. The ash content, representative of the mineral fraction, had an average of 3.46 g 100 g^{-1}, with a standard deviation of ±0.38 g 100 g^{-1}. On the other hand, the ether extract content was the most stable parameter, with an average of 1.10 g 100 g^{-1}, with a standard deviation of ±0.08 g 100 g^{-1}. In contrast, protein showed the greatest variability, with an average of 10.15 g 100 g^{-1} and a standard deviation of ±1.82 g 100 g^{-1}, suggesting differences in concentration at the different sampling points.

Table 5. Statistical summary of the carob fruit nutritional quality.

Properties	Mean	Maximum	Minimum	Standard Deviation (±)
Humidity (%)	12.11	13.61	10.38	0.74
Ash (g 100 g^{-1})	3.46	4.98	2.59	0.38
Ether extract (g 100 g^{-1})	1.10	1.27	0.90	0.08
Protein (g 100 g^{-1})	10.15	18.12	7.21	1.82

3.1.4. Vegetation Index Analysis

Figure 2 illustrates the box plots of the vegetation indices employed in this study. The RI index has the widest and most dispersed range of values, with a median close to 200 and outliers. Similarly, the RVI index also exhibits high dispersion, albeit on a smaller scale of values. The indices with a more compact distribution and centered around the median were GI (−0.26 ± 0.02), GVI (0.18 ± 0.02), S2 (−0.26 ± 0.03), S5 (0.30 ± 0.02), FI (1.75 ± 0.10), CI (1.53 ± 0.19), and SI (0.27 ± 0.04). On the other hand, the NDVI (0.39 ± 1.55), IPVI (0.69 ± 0.07), and NBR (0.24 ± 0.15) indices registered low values. However, their dispersion suggests variability in carob tree cover, possibly due to heterogeneity in canopy density or the presence of rainfall in some places.

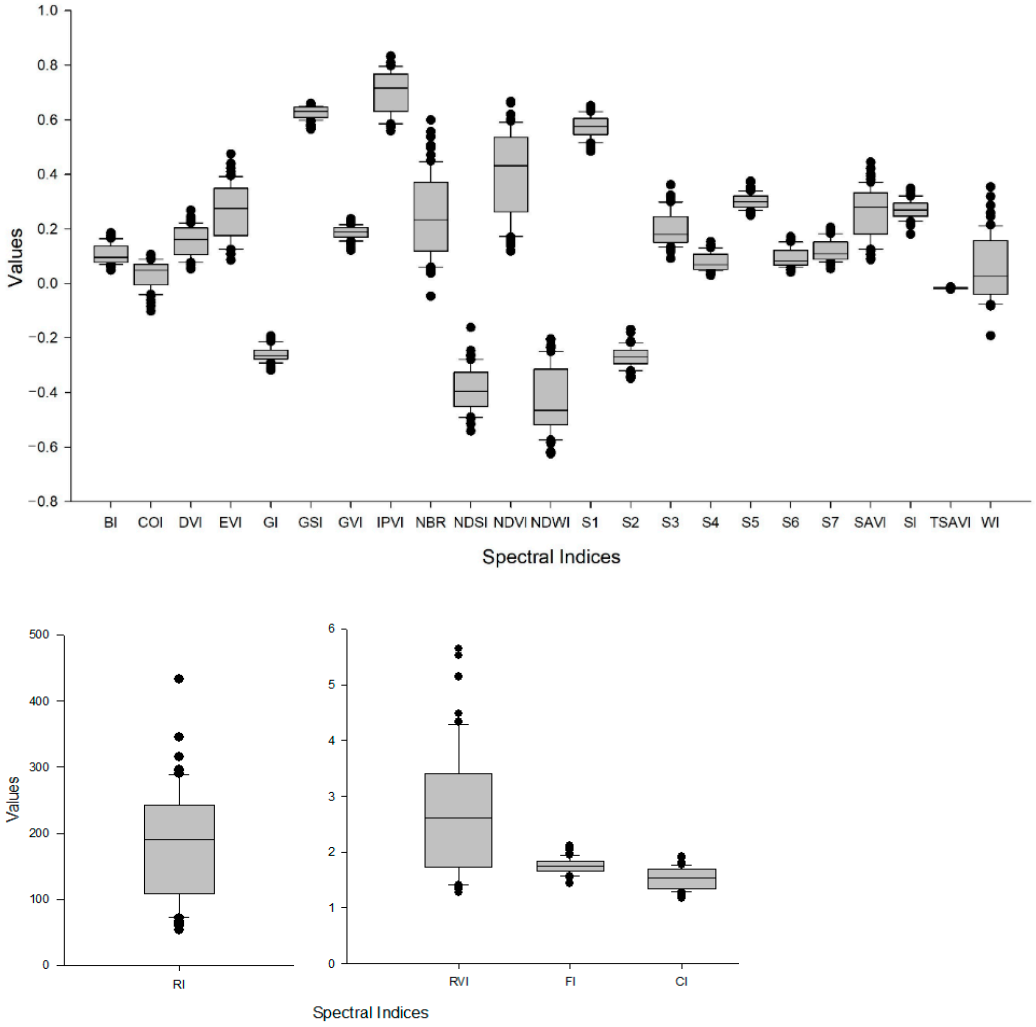

Figure 2. Variability in vegetation indices: Brightness Index (BI), Coloration Index (COI), Difference Vegetation Index (DVI), Enhanced Vegetation Index (EVI), Greenness Index (GI), Grain Size Index (GSI), Global Vegetation Index (GVI), Infrared Percentage Vegetation Index (IPVI), Normalized Burn Ratio (NBR), Normalized Difference Salinity Index (NDSI), Normalized Difference Vegetation Index (NDVI), Normalized Difference Water Index (NDWI), Salinity Index (S1, S2, S3, S4, S5, S6, and S7), Soil Adjusted Vegetation Index (SAVI), Saturation Index (SI), Transformed Soil Adjusted Vegetation Index (TSAVI) and Wetness Index (WI), Redness index (RI), Ratio Vegetation Index (RVI), Ferric Iron Index (FI), Clay Index (CI).

3.2. Relationship of Soil Physicochemical Properties and Vegetation Indices with the Protein and Ether Extract Content of Carob Fruit

3.2.1. Principal Component Analysis

Principal component analysis (Figure 3) reveals that proteins are positively correlated with the amount of ash and ether extract fat concentration but negatively correlated with moisture. Concerning soil physicochemical properties (Figure 3a), ether extract is associated with sand and total nitrogen (TN). On the other hand, the metals that present a greater relationship with ether extract and protein are selenium (Se) and antimony (Sb). Regarding vegetative indices, S1 and S2 show a positive correlation, while GVI and RI show a negative association with the ether extract concentration in carob. The first principal component (Dim1) in Figure 3a explains 19.6% of the variance, while the second principal component (Dim2) explains 14.5%, making a total of 34.1%. In the analysis of metals, the variance explained by the principal component (Dim1) is 55.4%, and that of the second component (Dim2) is 8.2%, totaling 63.6% (Figure 3b). In the case of vegetation indices, the explanation

of the variance by the principal component (Dim1) is 58.3%, and that of the secondary component is 14%, making a total of 72.3% (Figure 3c), which is the highest value.

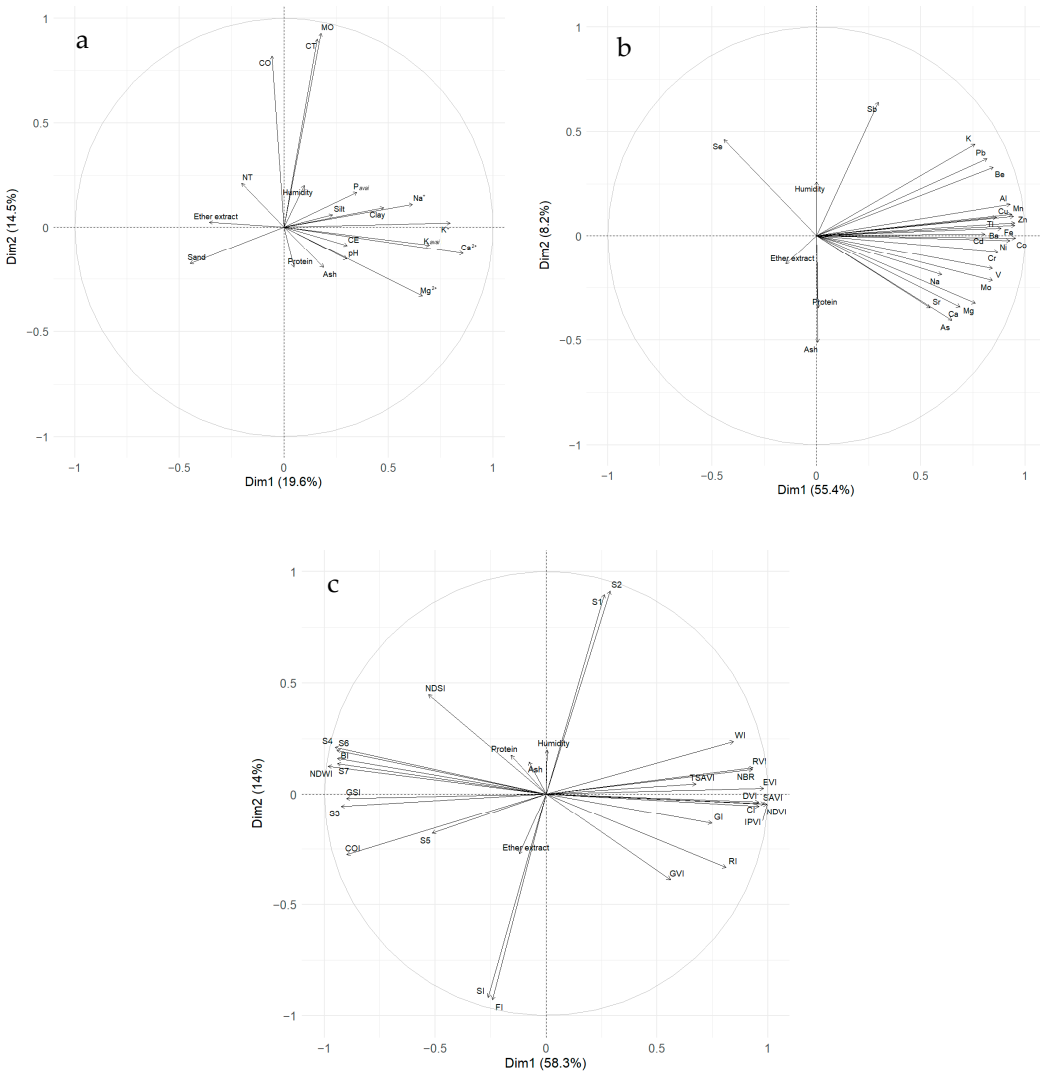

Figure 3. Principal component analysis for the different characteristics evaluated: (**a**) PCA for soil physicochemical properties, (**b**) PCA for metals in soil, and (**c**) PCA for vegetation indices.

3.2.2. Correlation of Proteins and Ether Extract with Soil Physicochemical Properties and Vegetation Indices

Figure 4 shows moderate positive correlations between protein and ash (CC =0.51) and ether extract (CC = 0.33), as well as a moderate negative correlation between moisture and ash (CC = −0.33). Other weak correlations also occur between ether extract and sand (CC = 0.22), antimony (CC = −0.28), calcium (CC = −0.26), and S5 (CC = −0.26). Protein shows weak correlations with pH (CC = 0.19) and NDSI (CC = 0.22). These results suggest that the chemical composition of carob is influenced by multiple factors, such as the percentage of sand, the pH, and the concentrations of some elements, such as Ca^{2+}, Sb, and Cu, with some associations being more significant than others.

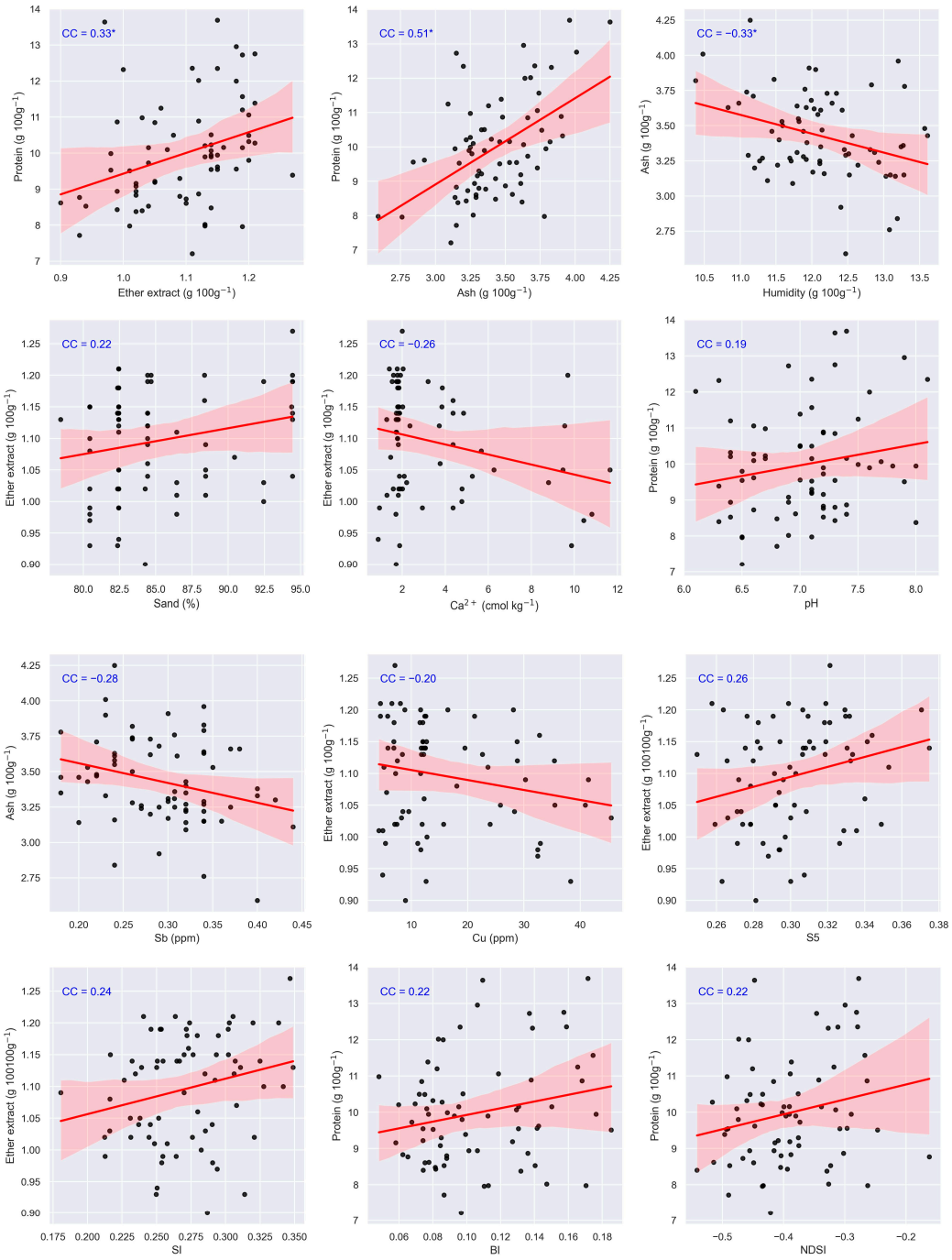

Figure 4. Relationship between ether extract, protein, ash, vegetation indices, and soil physicochemical factors. Red lines indicate the linear regression trend, and shaded red areas represent the 95% confidence intervals. Black points correspond to individual observations. * Significant differences are presented for a $p < 0.05$ (CC = correlation coefficient).

3.3. Predictive Modeling and Key Factor Analysis

The equations were obtained using the Eureqa-Formulize software (version 1.24.0), with carob fruit protein and ether extract fat as output variables and soil properties and vegetation indices as input variables. The selected equations presented the lowest margin of error and met the criteria for a good fit, as indicated by the statistical indicators shown in Figure 5. Table 6 presents the details of each selected equation. In the nonlinear multiple regression analysis, although the coefficient of determination (R^2) reflects the goodness

of the model fit, the other statistical indicators showed values within acceptable ranges, which supports the validity of the obtained fit.

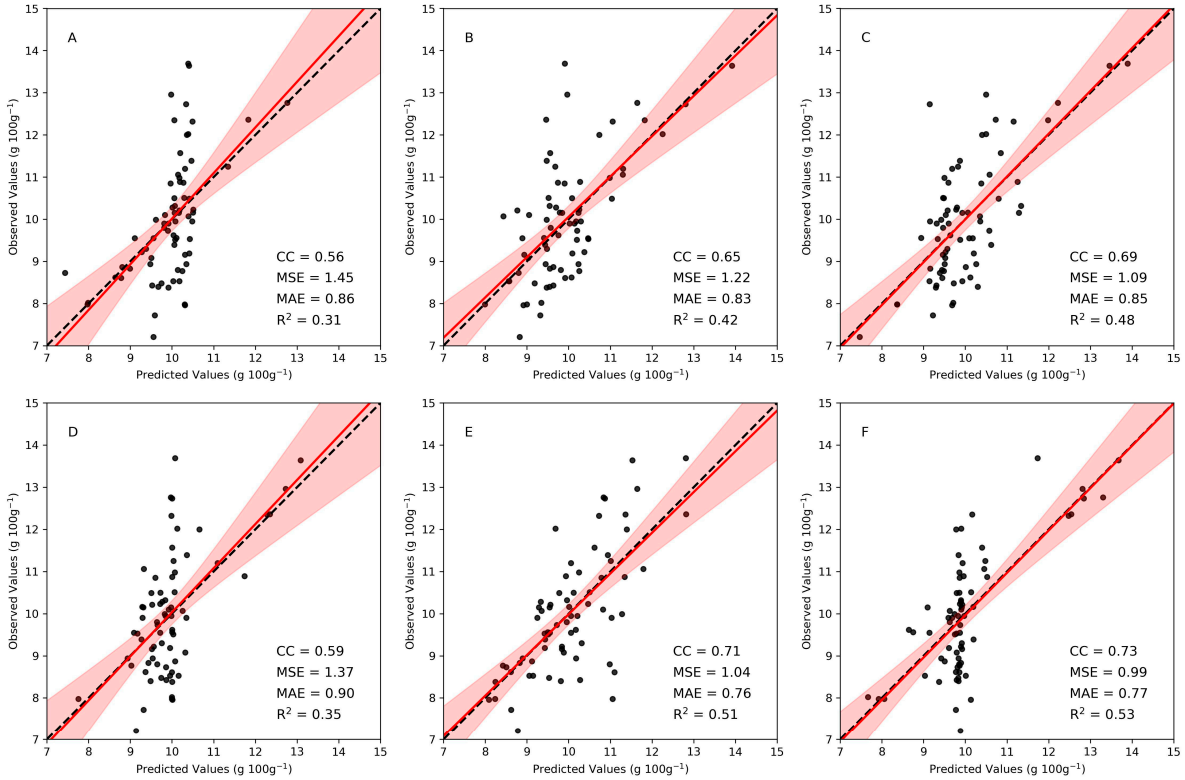

Figure 5. Relationship between the observed and predicted values for protein content using the linear models obtained with Eureqa-Formulize (the letters A, B, C, D, E, and F match the equations presented in Table 6 (A, B, C, D, E, and F)). Red lines indicate the linear regression trend, and shaded red areas represent the 95% confidence intervals. Black points correspond to individual observations.

Table 6. Protein and ether extract concentration prediction equations from soil properties and vegetation indices.

Model	ID	Equation
Protein	A	$11.20 + \frac{-7.59}{CE} + \frac{7.72}{(12.08-CE\times CT)} + \frac{-9.63}{137.52-21.99*CE)} - 0.008 \times CE - 0.01 \times CT \times P_{avai}$
	B	$11.52 + 2.63 \times Ca + 1.66 \times pH - \frac{192.01}{K_{avai}} + \frac{1.41}{K_{avai}-83.33} + 0.79 \times 10^{-9} \times Ca \times K_{avai}^3 - 0.37 \times Ca \times pH$
	C	$4.8 + \frac{-9.45}{Ash-5.26} + \frac{0.23}{0.103\times H\times Ash-5.25} + \frac{0.0678}{0.148\times H\times Ash-5.27} + \frac{-0.0366}{0.148\times H\times Ash^2-23.3}$
	D	$10.26 + \frac{-0.0001}{SAVI-0.33} + \frac{-0.00272}{0.32683-EVI} + \frac{-0.00692}{0.31115-EVI} + \frac{0.0003}{0.05419+SAVI^2-0.469\times SAVI} - 1.8892 \times EVI$
	E	$133.72 + WI + 82.13 \times S4 + 15.107 \times CI + 15.288 \times CI \times S3^2 \times COS(194.54 \times S5) - 19.24 - 69.90 \times CI \times WI - 319.98$
	F	$15.75 + \frac{0.015}{0.46-NDVI} - \frac{0.0039}{NDVI-0.161} + \frac{0.044}{0.1212+NDVI\times NDWI} + \frac{0.49-0.0058\times Sand}{BI-0.153} - 0.0688 \times Sand$
Ether extract	A′	$1.096 + 0.083 \times K + \frac{-0.019}{K\times Ca^4} + \frac{0.0025}{Ca-1.07-Ca\times K} + \frac{-0.0085}{0.226\times Sand-19.28-K} - 0.0022 \times Ca \times Silt$
	B′	$1.14 + \frac{-0.01}{0.226\times Sand-19.44} + \frac{0.0026}{Ca-1.23-Ca\times K} + \frac{0.0045\times Silt-0.0089}{Ca-1.277} - 0.0125 \times Silt$
	C′	$1.0769 + \frac{-0.0054}{Cu-0.0437\times Mn} + \frac{0.083\times Cu-0.62}{Co\times Cu-36.607} + \frac{292.7457}{Mn^2-3577.773-Co\times Cu\times Mn}$
	D′	$1.096 + \frac{0.0065-0.02\times S5}{28.075\times SI+26.61\times S2-0.44} + \frac{2.334\times SI-0.63}{18108.53+23.89\times S1+198866.95\times S5^2-120065.24\times S5} + \frac{3.066\times S5-0.926}{1191.97+13159.0147\times S5^2-26.606\times S2-7944.71\times S5}$
	E′	$1.096 + 0.083 \times COI \times RVI \times FI^3 + \frac{-0.0006}{3.415\times COI-18.14\times BI^2} - \frac{0.0000219}{0.009+BI\times COI-1.99\times BI^2} - 0.744 \times COI$
	F′	$1.05 + \frac{-0323}{Ca^2} + \frac{0.015\times Sand\times SI}{Ca} + \frac{-0.047\times NDVI}{3.11-0.0147\times Sand\times NDVI\times Ca^2} - SI \times NDVI^3$

where EC, electrical conductivity; Ca^{2+}, calcium ion; K_{avai}, potassium available; P_{avai}, phosphorus available; H, humidity; TC, total carbon; Mn, manganese; Cu, cupper; Co, cobalt; S1, S2, S3, S4, S5, salinity index; NDVI, Normalized Difference Vegetation Index; COI, Coloration Index; BI, Brightness Index; RVI, Ratio Vegetation Index; FI, Ferric Iron Index; NDWI, Normalized Difference Water Index; CI, Clay Index.

The prediction equations for protein content (Figure 5) in the algarroba obtained a coefficient of determination (R^2) in the range of 0.31 to 0.53, indicating a moderate predictive capacity. The correlation coefficient (CC) ranged from 0.53 to 0.73, while the mean squared error (MSE) ranged from 0.99 to 1.45, and the mean absolute error (MAE) ranged from 0.76 to 0.90. Among the equations evaluated, the one that presented the best performance was equation F, taking into account variables such as sand content, as well as the NDVI, NDWI, and BI indices. Equation F is better than E by 3.77% and 41.5% than equation A, taking into account R^2.

The prediction equations for the ether extract content (Figure 6) in carob yielded coefficients of determination (R^2) ranging from 0.37 to 0.46, indicating a moderate predictive capacity. The correlation coefficient (CC) ranged from 0.61 to 0.73, while the mean square error (MSE) was 0.004 and the mean absolute error (MAE) was 0.05 for all cases. Among the equations evaluated, those that showed the best performance were equations 6-B′ and 6-E′, considering variables such as silt, K, and calcium (Ca) content, as well as the RVI, FI, BI, and COI indices. Equations (B′) and (E′) are 2.17% higher than F′ and 19.56% higher than equation C′, considering R^2.

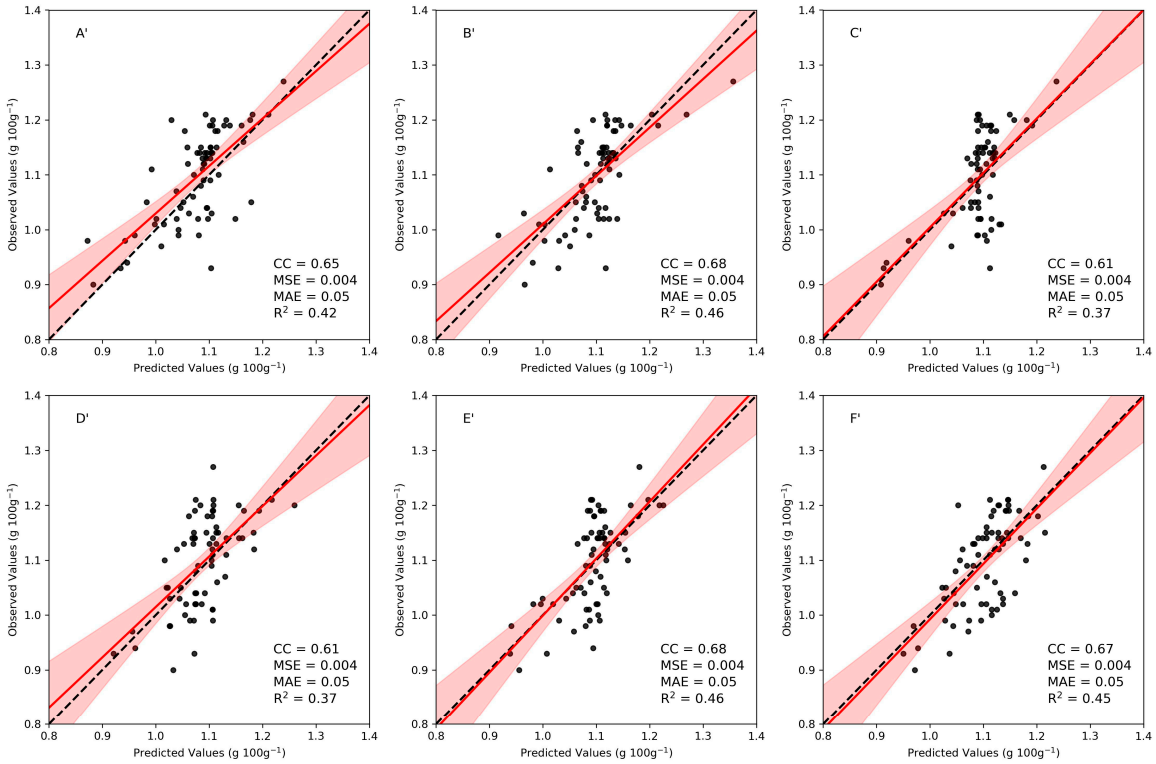

Figure 6. Relationship between observed and predicted values of ether extract content, using the linear models obtained with Eureqa-Formulize (The letters A′, B′, C′, D′, E′, and F′ correspond to the equations presented in Table 6 (A′, B′, C′, D′, E′, and F′)). Red lines indicate the linear regression trend, and shaded red areas represent the 95% confidence intervals. Black points correspond to individual observations.

4. Discussion

4.1. Soil Physicochemical Characterization

The analyzed soils exhibit significant variability in their physicochemical properties, which may impact the productivity of the dry forest ecosystem in northern Peru. The carob *Neltuma* spp. thrives in arid, semi-arid, tropical, and subtropical regions, in saline and alkaline soils [67], as reported in this study, due to the lack of rainfall. Low levels of available phosphorus are present, which can limit the growth and development of carob,

affecting root formation and the efficiency of water and nutrient absorption [68]. The average organic matter content indicates the good capacity of the soil to retain moisture and nutrients, being 30% higher than that reported by [69]. Soil texture is dominated by the sandy fraction, with a maximum of 98.44% and a minimum of 38.29%, similar to those reported by [70], who found 96.4% sand. *Neltuma* species are resistant to water scarcity and tolerant to salinity [71]. These characteristics allow it to grow in the semi-arid zone of Peru, with minimal soil nutrient requirements. The physicochemical properties of the soil, such as the percentage of sand and the pH, had the highest correlations with the concentration of ether extract and protein, respectively. In the case of pH, it aligns with the study by [72] that examines the variation in nutritional quality of grapefruit. The texture of the soil and the content of microelements modify the nutritional quality of the seed oil of an edible halophyte [73]. Nitrogen (N) is also an essential element of amino acids (proteins); its deficiency reduces leaf growth and pod productivity [74]. Like nitrogen, potassium (K) is a primary macronutrient for plants, and it regulates key enzymatic functions involved in metabolism and protein synthesis [75]. Together with N and K, the other macronutrient phosphorus (P) had lower correlations than those found by [76] between available phosphorus and protein content in potato crops.

4.2. Potential for Heavy Metal Pollution in the Soil Where the Carob Tree Grows

The concentrations of arsenic (As), nickel (Ni), lead (Pb), and cadmium (Cd) in the soil samples were within the permissible limits established by the World Health Organization (WHO). Similar results were reported by [77], with the following values found in soils: Ni = 466.256 > Pb = 12.009 > As = 5.486 > Cd = 0.394 mg kg^{-1}, reversing the order of Ni, As, and Pb. However, Cr concentrations exceeded the limits allowed by the WHO, as they were present in 84.4% of the samples. The presence of trees favors the immobilization of cadmium in soils, as indicated by [78], who found higher cadmium contents in soils with trees than in soils without trees; this is due to the density of the trees. The high presence of heavy metals in soils causes intoxication and, in agricultural soils, poses a serious risk to plant life, human health, and the global food supply, with negative implications for both health and crop yields [79]. Therefore, it is necessary to study the concentration of metals in carob to rule out that these are translocated from the soil to the fruit. The highest correlations found in this study are between Sb and ash and between Cu and ether extract; the other metals do not present correlations greater than 0.20. [80] found that there is a strong mobility of metals from the soil to fresh fruits, especially in areas with low CEC values. However, it has also been demonstrated that the highest concentration of heavy metals is found in the root system, rather than in the aerial components of the plant [81].

4.3. Proximal Composition of Carob

The results obtained for ether extract and protein are 20% and 30% higher than those reported by [9]; as for ash content, the values are similar. Regarding the ash content, no significant differences were observed. When comparing the ether extract content with total lipids, it is observed that ether extract is lower by 43.3%, 60.6%, and 50.5% compared to *Prosopis alba*, *Prosopis chilensis* (yellow), and *P. chilensis* (brown) flour, respectively [82]. Compared to the previous study, the protein content was 28.8% and 6.8% higher than *P. alba* and *P. chilensis* (yellow) but 5.9% lower compared to *P. chilensis* (brown). These high values of protein and ether extract content have led to the flour of various species of Neltuma being used as an alternative to improve the nutritional quality of certain products [83]. Knowing the concentrations from soil characteristics or spectral indices will enable the accurate implementation and development of these products at a lower cost. Additionally, the use of vegetation indices facilitates the observation of spatial variations, which can

optimize decision-making in the management and production of carob trees. It can help in the prediction of yields [84], the detection of stress disputes [85] and, in this case, the prediction of protein and ether extract.

4.4. Carob Vegetation Indices

In general, the values of the spectral indices are low, which aligns with the findings of [29] for the visible spectrum. Meanwhile, the near-infrared values tend to be higher, depending on the time of year. These values can also be affected by wet or dry periods. In denser forests, NDVI values can exceed 0.5, although they are typically around 0.4 on average, as reported by [27,29]. The same study indicates that EVI values range from 0.14 to 0.20, although during wet periods, they can reach values of up to 0.5. In this study, the average value recorded is 0.27, which is close to the expected range, considering that these values only represent those of the carob tree. The use of vegetation indices obtained from satellite imagery has been widely applied in different studies, including the early prediction of protein and oil in soybean cultivation with an RMSE of 1.804 and 1.04, respectively [86].

4.5. Forecasting of the Protein and Ether Extract Content from Soil Physicochemical Properties

The values obtained for R^2 in the equations generated are similar to those reported by [72], who achieved an R^2 of 0.50 and an MAE of 0.0003 in the prediction of the nutritional quality of grapefruit using a random forest model. In that study [72], the most important variables were pH, calcium, potassium, magnesium ions, and soil organic matter, coinciding in part with the most relevant variables in this study (pH, calcium, and potassium ions). Although studies on the prediction of protein content regarding soil properties are scarce, some research relates the yield to soil quality indices. For example, with regard to apple trees, [87] reported an R^2 of 0.56. Likewise, [76] estimated the soluble protein content in potatoes with an R^2 of 0.32, a value lower than the maximum values obtained in this study (R^2 = 0.53). However, both models highlight the importance of variables such as potassium, available phosphorus, and pH. In addition, [17] employed artificial neural network models to predict peach fruit quality through the calcium, potassium, nitrogen, and manganese content in the soil.

4.6. Prediction of Protein and Ether Extract Content from Vegetation Indices

Although no specific studies have been found on the prediction of protein content in *Neltuma*, previous research has shown that the near-infrared region allows information on compounds such as phospholipids and phosphoproteins in plants [88]. Within this spectrum, vegetation indices such as NDVI and NDWI are found, which, in the present research, were representative in the generated equations. Previous studies have reported R^2 values greater than 0.60 for predicting the protein content using NDVI [89–91]. These results are supported by [92], who used multispectral images obtained with unmanned aerial vehicles. Other indices, such as RVI, have also been used in predicting protein content [93]. However, information on estimating lipid concentration in fruit trees from soil properties and vegetation indices remains limited. In this context, research has shown that multispectral reflectance in the range of 460 to 1680 nm allows for the prediction of lipid content in pastures, with R^2 values between 0.60 and 0.80 [94]. In this spectral range, the vegetation indices are used to generate models of ether extract content in the algae sheath in the present research. Likewise, these remote sensing techniques have been applied to estimate the carbon-nitrogen ratio in grasslands [95].

The prediction of the ether extract and protein content in carob fruit from soil physicochemical properties and vegetation indices aims to support the more accurate estimation of these nutritional components. The predictive equations developed in this study incorporate multiple variables and terms. However, the complexity of these models could be refined

with a larger sample size, which would likely reduce the number of variables required and improve the R^2 and CC values, thereby enhancing model performance. It is essential to note that carob production occurs within a natural system, with minimal human intervention in management practices. Future research could explore the impact of specific management practices on soil quality and carob productivity. Additionally, incorporating functional biodiversity analyses would be valuable to provide a deeper understanding of the interactions among soil properties, vegetation, soil biota, and the ecosystem services provided by dry forests.

The findings of this study contribute to the sustainability of dry forests by demonstrating that the nutritional quality of carob, specifically their protein and ether extract content, is influenced by the specific physicochemical properties of the soil. This finding highlights the importance of integrated ecosystem management, where soil conservation is recognized as an essential component for maintaining the productivity and ecological functionality of these forests. The assessment of protein and ether extract concentrations supports the valorization of carob as a strategic food resource for local communities and livestock systems, thereby strengthening food security and promoting the sustainable use of native species. Furthermore, the application of vegetation indices derived from remote sensing enables the generation of spatial information regarding the nutritional quality of carob fruit. This approach offers new possibilities for monitoring the impacts of climate change [96] on carob yield, estimating the ecosystem's energy contribution, and determining the livestock carrying capacity within forested areas. Collectively, these findings position the study as a valuable tool for supporting evidence-based ecological restoration strategies [97] and guiding the sustainable management of natural resources in dry forest ecosystems.

5. Conclusions

The results of this study provide insight into the influence of soil physicochemical properties, metal concentrations, and vegetation indices on the protein and ether extract concentrations of the carob tree (*Neltuma*) fruit in the dry forest of the northern coast of Peru. The soil characterization results indicate a texture with an average of 84.68% and a standard deviation of ±7.31%. The protein and ether extract content of carob is 10.15 g 100 g^{-1} ± 1.82 g 100 g^{-1} and 1.10 g 100 g^{-1} ± 0.08 g 100 g^{-1}, constituting an important source for feeding goats and sheep. In the case of metals in the soil, the Cr content exceeds the levels suggested by the WHO. This is an issue that should be addressed in future studies to rule out its presence in carob. There are correlations between the ether extract and the percentage of sand (0.22), Ca+2 (−0.26), Cu (−0.20), S5 (0.26), and Si (0.24). In the case of the protein, correlations are observed with pH (r = 0.19), BI (r = 0.22), and NDSI (r = 0.22).

In the development of predictive equations for protein concentration, Equation F demonstrated the best performance, with an R^2 of 0.53 between the observed and predicted values, representing a 41.5% improvement over the lowest-performing equation, which had an R^2 of 0.31. The variables contributing to this model were NDVI, NDWI, BI, and sand content. For ether extract prediction, two equations, B′ and E′, were identified as the most effective, both achieving an R^2 of 0.46, with an MSE of 0.004 and an MAE of 0.05. The key predictive variables in these models included sand, potassium, calcium ions, and the vegetation indices (VIs): COI, RVI, BI, and FI. In both protein and ether extract models, sand content and the BI vegetation index consistently emerged as significant predictors. These equations should be considered as initial baselines, and their predictive accuracy could be substantially improved by increasing the sample size and incorporating sampling points from other regions. Additionally, the application of more advanced modelling approaches, such as machine learning algorithms, may further enhance the predictive accuracy. Monitoring the protein and ether extract concentrations in Neltuma pallida

(carob) fruit using soil physicochemical properties and vegetation indices offers a more accessible approach and contributes to its sustainable utilization. These findings aim to strengthen the integrated management of the dry forest ecosystem and to enhance the valorization of carob as a vital food resource for local communities.

Author Contributions: Conceptualization, R.S. and W.S.; methodology, W.S. and C.C.-G.; software, W.S.; validation, W.S. and C.C.-G.; formal analysis, W.S.; investigation, R.S., D.G.-P., C.V.-d.-l.-C., R.R., and S.L.; resources, J.C. and R.S.; data curation, W.S.; writing—original draft preparation, C.C.-G. and W.S.; writing—review and editing, D.G.-P., R.R., E.S., and R.S.; visualization, W.S.; supervision, R.S.; project administration, R.S. and J.C.; funding acquisition, J.C. All authors have read and agreed to the published version of the manuscript.

Funding: This research was funded by the CUI 2487112 INIA project "Mejoramiento de los servicios de investigación y transferencia tecnológica en el manejo y recuperación de suelos agrícolas degradados y aguas para riego en la pequeña y mediana agricultura en los departamentos de Lima, Áncash, San Martín, Cajamarca, Lambayeque, Junín, Ayacucho, Arequipa, Puno y Ucayali" and CONCYTEC—Project N°PE501082832-2023-PROCIENCIA "Caracterización metagenómica de la microbiota de la cabra y su efecto sobre el perfil metabolómico de un fermentado a base de alga-rrobo de la región Piura" and Project "Mejoramiento de los servicios de investigación y transferencia tecnológica en el manejo y recuperación de suelos agrícolas degradados y aguas para riego en la pequeña y mediana agricultura en los departamentos de Lima, Áncash, San Martín, Cajamarca, Lambayeque"—CUI 2487112 INIA.

Institutional Review Board Statement: Not applicable.

Informed Consent Statement: Not applicable.

Data Availability Statement: Data are contained within the article.

Acknowledgments: The authors thank the technology transfer specialists from the Proyecto PROCAP Piura, who supported the collection of field samples.

Conflicts of Interest: The authors declare no conflicts of interest.

References

1. Quiroga, J.A.; Roa, H.Y.; Melo, O.; Fernández, F. Estructura de fragmentos de bosque seco tropical en el sur del departamento del Tolima, Colombia. *Bol. Cient. Mus. Hist. Nat. Univ. Caldas* **2019**, *23*, 31–51. [CrossRef]
2. Padrón, E.; Padrón, E.; Navarro Cerrillo, R.M. Aboveground Biomass in Prosopis Pallida (Humb. and Bonpl. Ex Willd.) H. B. K. Ecosystems Using Landsat 7 ETM Images. *Rev. Chil. Hist. Nat.* **2007**, *80*, 43–53. Available online: https://www.biodiversitylibrary.org/part/116663 (accessed on 20 March 2025). [CrossRef]
3. Servicio Nacional Forestal y de Fauna Silvestre (SERFOR). Avances sobre la investigación de Algarrobo—Prosopis (Fabaceae) en la Costa Norte del Perú. *SERFOR-Institucional* **2021**, *71*, 317–324.
4. Cuentas Romero, M.A.; Salazar Toledo, A.Í. De la especie al ecosistema; del ecosistema a la sociedad: Revalorizando el algarrobo (ProsoPis Pallida) y el reto de su conservación en Lambayeque y en la costa norte del Perú. *Espacio Desar.* **2017**, *30*, 129–159. [CrossRef]
5. Depenthal, J.; Meitzner Yoder, L.S. Community Use and Knowledge of Algarrobo (Prosopis Pallida) and Implications for Peruvian Dry Forest Conservation. *Rev. Ambientales.* **2018**, *52*, 49–70. [CrossRef]
6. Dostert, N.; Dostert, N.; Weigend, M.; Roque, J.; Cano, A.; La Torre Acuy, M.I.; Brokamp, G.; Flores, D. Siete Especies de Plantas Vasculares de Importancia Económica en el Perú: Fichas botánicas. *Arnaldoa* **2015**, *20*, 359–432.
7. Silva, M.; Martinez, M.J.; Coirini, R.; Brunetti, M.A.; Balzarini, M.; Karlin, U. Valoración Nutritiva Del Fruto Del Algarrobo Blanco (Prosopis Chilensis) Bajo Distintos Tipos de Almacenamiento. *Multequina* **2000**, *9*, 65–74.
8. Servicio Nacional Forestal y de Fauna Silvestre (SERFOR). En El Día de La Algarrobina, Serfor Hace Un Llamado Para Articular Esfuerzos Frente a La Tala Ilegal Indiscriminada Del Algarrobo—Noticias—Servicio Nacional Forestal y de Fauna Silvestre—Plataforma Del Estado Peruano. Available online: https://www.gob.pe/institucion/serfor/noticias/1126293-en-el-dia-de-la-algarrobina-serfor-hace-un-llamado-para-articular-esfuerzos-frente-a-la-tala-ilegal-indiscriminada-del-algarrobo (accessed on 11 April 2025).

9. Grados, N.; Cruz, G.; Albán, L.; Felker, P. Peruvian Prosopis Pallida: Its Potential to Provide Human and Livestock Food for Tropical Arid Lands of the World. In *Prosopis as a Heat Tolerant Nitrogen Fixing Desert Food Legume: Prospects for Economic Development in Arid Lands*; Puppo, M.C., Felker, P., Eds.; Academic Press: Cambridge, MA, USA, 2022; pp. 241–251, ISBN 978-0-12-823320-7. [CrossRef]
10. Giombolini, K.J.; Chambers, K.J.; Schlegel, S.A.; Dunne, J.B. Testing the Local Reality: Does the Willamette Valley Growing Region Produce Enough to Meet the Needs of the Local Population? A Comparison of Agriculture Production and Recommended Dietary Requirements. *Agric. Hum. Values* **2011**, *28*, 247–262. [CrossRef]
11. Scheelbeek, P.F.D.; Moss, C.; Kastner, T.; Alae-Carew, C.; Jarmul, S.; Green, R.; Taylor, A.; Haines, A.; Dangour, A.D. United Kingdom's Fruit and Vegetable Supply Is Increasingly Dependent on Imports from Climate-Vulnerable Producing Countries. *Nat. Food* **2020**, *1*, 705–712. [CrossRef]
12. Jiang, Y.; Zeng, Q.; Wei, J.; Jiang, J.; Li, Y.; Chen, J.; Yu, H. Growth, Fruit Yield, Photosynthetic Characteristics, and Leaf Microelement Concentration of Two Blueberry Cultivars under Different Long-Term Soil pH Treatments. *Agronomy* **2019**, *9*, 357. [CrossRef]
13. Ye, L.; Zhao, X.; Bao, E.; Li, J.; Zou, Z.; Cao, K. Bio-Organic Fertilizer with Reduced Rates of Chemical Fertilization Improves Soil Fertility and Enhances Tomato Yield and Quality. *Sci. Rep.* **2020**, *10*, 177. [CrossRef] [PubMed]
14. McCray, J.M.; Ji, S.; Powell, G. Sugarcane Yield Response to Potassium Fertilization as Related to Extractable Soil Potassium on Florida Histosols. *Agron. J.* **2017**, *109*, 2243–2252. [CrossRef]
15. Chen, X.; Yan, X.; Muneer, M.A.; Weng, X.; Cai, Y.; Ma, C.; Liu, Y.; Zhang, S.; Zhang, W.; Yang, W.; et al. Pomelo Green Production on Acidic Soil: Reduce Traditional Fertilizers, but Do Not Ignore Magnesium. *Front. Sustain. Food Syst.* **2022**, *6*, 948810. [CrossRef]
16. Loekito, S.; Afandi; Afandi, A.; Nishimura, N.; Koyama, H.; Senge, M. The Effects of Calcium Fertilizer Sprays during Fruit Development Stage on Pineapple Fruit Quality under Humid Tropical Climate. *Int. J. Agron.* **2022**, *2022*, 3207161. [CrossRef]
17. Sun, H.; Huang, X.; Chen, T.; Zhou, P.; Huang, X.; Jin, W.; Liu, D.; Zhang, H.; Zhou, J.; Wang, Z.; et al. Fruit Quality Prediction Based on Soil Mineral Element Content in Peach Orchard. *Food Sci. Nutr.* **2022**, *10*, 1756–1767. [CrossRef]
18. Zhang, Q.; Li, M.; Zhou, B.; Zhang, J.; Wei, Q. Quantitative Analysis of Relationship Between Fruit Quality of 'Fuji' Apple and Environmental Factors: A Case Study of the Loess Plateau Production Region. *Erwerbs-Obstbau* **2023**, *65*, 423–434. [CrossRef]
19. Shao, Z.; Li, C.; Li, D.; Altan, O.; Zhang, L.; Ding, L. An Accurate Matching Method for Projecting Vector Data into Surveillance Video to Monitor and Protect Cultivated Land. *ISPRS Int. J. Geo-Inf.* **2020**, *9*, 448. [CrossRef]
20. Angelopoulou, T.; Chabrillat, S.; Pignatti, S.; Milewski, R.; Karyotis, K.; Brell, M.; Ruhtz, T.; Bochtis, D.; Zalidis, G. Evaluation of Airborne HySpex and Spaceborne PRISMA Hyperspectral Remote Sensing Data for Soil Organic Matter and Carbonates Estimation. *Remote Sens.* **2023**, *15*, 1106. [CrossRef]
21. Sahbeni, G.; Ngabire, M.; Musyimi, P.K.; Székely, B. Challenges and Opportunities in Remote Sensing for Soil Salinization Mapping and Monitoring: A Review. *Remote Sens.* **2023**, *15*, 2540. [CrossRef]
22. Weiss, M.; Jacob, F.; Duveiller, G. Remote Sensing for Agricultural Applications: A Meta-Review. *Remote Sens. Environ.* **2020**, *236*, 111402. [CrossRef]
23. Bastos, L.M.; Froes de Borja Reis, A.; Sharda, A.; Wright, Y.; Ciampitti, I.A. Current Status and Future Opportunities for Grain Protein Prediction Using On- and Off-Combine Sensors: A Synthesis-Analysis of the Literature. *Remote Sens.* **2021**, *13*, 5027. [CrossRef]
24. Ryu, C.; Suguri, M.; Iida, M.; Umeda, M.; Lee, C. Integrating Remote Sensing and GIS for Prediction of Rice Protein Contents. *Precis. Agric.* **2011**, *12*, 378–394. [CrossRef]
25. Xu, X.; Zhou, L.; Taylor, J.; Casa, R.; Fan, C.; Song, X.; Yang, G.; Huang, W.; Li, Z. The 500-Meter Long-Term Winter Wheat Grain Protein Content Dataset for China from Multi-Source Data. *Sci. Data* **2024**, *11*, 1025. [CrossRef] [PubMed]
26. Farifteh, J.; Van der Meer, F.; Atzberger, C.; Carranza, E.J.M. Quantitative Analysis of Salt-Affected Soil Reflectance Spectra: A Comparison of Two Adaptive Methods (PLSR and ANN). *Remote Sens. Environ.* **2007**, *110*, 59–78. [CrossRef]
27. Vera, E.; Cruz, C.; Barboza, E.; Salazar, W.; Canta, J.; Salazar, E.; Vásquez, H.V.; Arbizu, C.I. Change of Vegetation Cover and Land Use of the Pómac Forest Historical Sanctuary in Northern Peru. *Int. J. Environ. Sci. Technol.* **2024**, *21*, 8919–8930. [CrossRef]
28. Barboza, E.; Bravo, N.; Cotrina-Sanchez, A.; Salazar, W.; Gálvez-Paucar, D.; Gonzales, J.; Saravia, D.; Valqui-Valqui, L.; Cárdenas, G.P.; Ocaña, J.; et al. Modeling the Current and Future Habitat Suitability of Neltuma Pallida in the Dry Forest of Northern Peru under Climate Change Scenarios to 2100. *Ecol. Evol.* **2024**, *14*, e70158. [CrossRef]
29. Aldana, C.; Lloret, J.; Moncada, W.; Rojas Acuña, J.; Saavedra, Y.; Tirado-Kulieva, V.A. Un Nuevo Algoritmo Para Determinar La Cobertura Espacial Del Algarrobo (Neltuma Piurensis) Por Piso Ecológico: Caso de La Cuenca Del Río Chira-Piura. *Remote Sens. Appl. Soc. Environ.* **2024**, *36*, 101363. [CrossRef]
30. Barboza, E.; Salazar, W.; Gálvez-Paucar, D.; Valqui-Valqui, L.; Valqui, L.; Zagaceta, L.H.; Gonzales, J.; Vásquez, H.V.; Arbizu, C.I. Cloud Computing Application for the Analysis of Land Use and Land Cover Changes in Dry Forests of Peru. *IJEI* **2024**, *7*, 505–514. [CrossRef]

31. Corredor, F.-A.; Figueroa, D.; Estrada, R.; Burgos-Paz, W.; Salazar, W.; Cruz, W.; Lobato, R.; Injante, P.; Godoy, D.; Barrantes, C.; et al. Genome-Wide Single Nucleotide Polymorphisms Reveal the Genetic Diversity and Population Structure of Creole Goats from Northern Peru. *Livest. Sci.* **2024**, *283*, 105473. [CrossRef]
32. *Method 9045D*; Soil and Waste pH, Revision 4. United States Environmental Protection Agency (USEPA): Washington, DC, USA, 2004. Available online: https://www.epa.gov/sites/default/files/2015-12/documents/9045d.pdf (accessed on 1 June 2025).
33. *ISO 11265:1994*; Soil Quality—Determination of the Specific Electrical Conductivity. ISO (International Organization for Standardization): Geneva, Switzerland, 1994. Available online: https://www.iso.org/standard/19243.html (accessed on 1 June 2025).
34. Walkley, A.; Black, I.A. An Examination of the Degtjareff Method for Determining Soil Organic Matter, and a Proposed Modification of the Chromic Acid Titration Method. *Soil. Sci.* **1934**, *37*, 29–38. [CrossRef]
35. *Norma Oficial Mexicana que Establece las Especificaciones de Fertilidad, Salinidad y Clasificación de Suelos*. Secretaría de Medio Ambiente y Recursos Naturales (SEMARNAT): Estudios, Muestreo y Análisis. 2002. Available online: https://faolex.fao.org/docs/pdf/mex50674.pdf (accessed on 1 June 2025).
36. *ISO 13878:1998*; International Organization for Standardization (ISO). Soil Quality—Determination of Total Nitrogen by Dry Combustion (Elemental Analysis); First Edition. ISO: Geneva, Switzerland, 1998.
37. United States Environmental Protection Agency (USEPA), Method 6020B: Inductively Coupled Plasma–Mass Spectrometry. Revision 2, 2014. Washington, DC, USA. Available online: https://www.epa.gov/sites/default/files/2015-12/documents/6020b.pdf (accessed on 1 June 2025).
38. *NTP 208.017:2021*; Cacao y Chocolate—Determinación de Humedad. Método Gravimétrico, 4ª ed. Instituto Nacional de Calidad (INACAL): Lima, Perú, 2021.
39. *NTP 208.016:2021*; Cacao y Chocolate—Grasa en Productos del Cacao. Método de Extracción por Soxhlet, 4ª ed. Instituto Nacional de Calidad (INACAL): Lima, Perú, 2021.
40. *Official Method 2001.11*; Protein (Crude) in Animal Feed, Forage (Plant Tissue), Grain, and Oilseeds—Block Digestion Method Using Copper Catalyst and Steam Distillation into Boric Acid; Edition 2023. AOAC International: Rockville, MD, USA, 2023.
41. *Official Method 930.05*; Ash of Plants, Chapter 3; 22nd ed. AOAC International: Rockville, MD, USA, 2023.
42. Markert Restee Documentation. Available online: https://kmarkert.github.io/restee/ (accessed on 11 April 2025).
43. Wu, Q. Geemap: A Python Package for Interactive Mapping with Google Earth Engine. *Open Source Softw.* **2020**, *5*, 2305. [CrossRef]
44. Van den Bossche, J.; Journois, M.; Jordahl, K.; Wolf, L.J.; Fernandes, F.; Farmer, C.; Ward, B.; Perry, M.; Farmer, C.; Hjelle, G.A.; et al. GeoPandas: The Geospatial Data Library for Python, Version 0.13.2. Zenodo 2023. Available online: https://doi.org/10.5281/zenodo.8009629 (accessed on 1 June 2025).
45. Khan, N.M.; Rastoskuev, V.V.; Sato, Y.; Shiozawa, S. Assessment of Hydrosaline Land Degradation by Using a Simple Approach of Remote Sensing Indicators. *Agric. Water Manag.* **2005**, *77*, 96–109. [CrossRef]
46. Mathieu, R.; Pouget, M.; Cervelle, B.; Escadafal, R. Relationships between Satellite-Based Radiometric Indices Simulated Using Laboratory Reflectance Data and Typic Soil Color of an Arid Environment. *Remote Sens. Environ.* **1998**, *66*, 17–28. [CrossRef]
47. Tucker, C.J. Red and Photographic Infrared Linear Combinations for Monitoring Vegetation. *Remote Sens. Environ.* **1979**, *8*, 127–150. [CrossRef]
48. Anand, A.; Pandey, P.; Petropoulos, G.; Pavlidés, A.; Srivastava, P.; Sharma, J.; Malhi, R. Uso de Hyperion para la evaluación de las reservas de carbono de los bosques de manglares en la reserva forestal de Bhitarkanika: Una contribución a la iniciativa del carbono azul. *Remote Sens.* **2020**, *12*, 597. [CrossRef]
49. Gitelson, A.A.; Kaufman, Y.J.; Merzlyak, M.N. Use of a Green Channel in Remote Sensing of Global Vegetation from EOS-MODIS. *Remote Sens. Environ.* **1996**, *58*, 289–298. [CrossRef]
50. Xiao, J.; Shen, Y.; Tateishi, R.; Bayaer, W. Development of Topsoil Grain Size Index for Monitoring Desertification in Arid Land Using Remote Sensing. *Int. J. Remote Sens.* **2006**, *27*, 2411–2422. [CrossRef]
51. Kidwell, K.B. *Global Vegetation Index User's Guide, Revised October 1990*; U.S. Department of Commerce, National Oceanic and Atmospheric Administration, National Environmental Satellite Data and Information Service, National Climatic Data Center, Satellite Data Services Division: Washington, DC, USA, 1990.
52. Crippen, R.E. Calculating the Vegetation Index Faster. *Remote Sens. Environ.* **1990**, *34*, 71–73. [CrossRef]
53. Roy, D.P.; Boschetti, L.; Trigg, S.N. Remote Sensing of Fire Severity: Assessing the Performance of the Normalized Burn Ratio. *IEEE Geosci. Remote Sens. Lett.* **2006**, *3*, 112–116. [CrossRef]
54. Nguyen, K.; Liou, Y.; Tran, H.; Hoang, P.; Nguyen, T. Soil salinity assessment by using near-infrared channel and Vegetation Soil Salinity Index derived from Landsat 8 OLI data: A case study in the Tra Vinh Province, Mekong Delta, Vietnam. *Prog. Earth Planet. Sci.* **2020**, *7*, 1–16. [CrossRef]
55. Rouse, J.W.; Haas, R.H.; Schell, J.A.; Deering, D.W. Monitoring Vegetation Systems in the Great Plains with ERTS. *NASA Spec. Publ.* **1974**, 309–317.
56. Choudhury, B.J.; Golus, R.E. Estimating soil wetness using satellite data. *Int. J. Remote Sens.* **1988**, *9*, 1251–1257. [CrossRef]

57. Bannari, A.; Guedon, A.M.; El-Harti, A.; Cherkaoui, F.Z.; El-Ghmari, A. Characterization of Slightly and Moderately Saline and Sodic Soils in Irrigated Agricultural Land Using Simulated Data of Advanced Land Imaging (EO-1) Sensor. *Commun. Soil Sci. Plant Anal.* **2008**, *39*, 2795–2811. [CrossRef]
58. Taghizadeh-Mehrjardi, R.; Schmidt, K.; Toomanian, N.; Heung, B.; Behrens, T.; Mosavi, A.; Band, S.S.; Amirian-Chakan, A.; Fathabadi, A.; Scholten, T. Improving the Spatial Prediction of Soil Salinity in Arid Regions Using Wavelet Transformation and Support Vector Regression Models. *Geoderma* **2021**, *383*, 114793. [CrossRef]
59. Douaoui, A.E.K.; Nicolas, H.; Walter, C. Detecting Salinity Hazards within a Semiarid Context by Means of Combining Soil and Remote-Sensing Data. *Geoderma* **2006**, *134*, 217–230. [CrossRef]
60. Huete, A.R. A Soil-Adjusted Vegetation Index (SAVI). *Remote Sens. Environ.* **1988**, *25*, 295–309. [CrossRef]
61. Baret, F.; Guyot, G.; Major, D.J. TSAVI: A Vegetation Index Which Minimizes Soil Brightness Effects On LAI And APAR Estimation. In Proceedings of the 12th Canadian Symposium on Remote Sensing, Vancouver, BC, Canada, 10–14 July 1989; IEEE: Piscataway, NJ, USA, 1989; Volume 3, pp. 1355–1358.
62. Major, D.J.; Baret, F.; Guyot, G. A ratio vegetation index adjusted for soil brightness. *Int. J. Remote Sens.* **1990**, *11*, 727–740. [CrossRef]
63. John, K.; Abraham Isong, I.; Michael Kebonye, N.; Okon Ayito, E.; Chapman Agyeman, P.; Marcus Afu, S. Using Machine Learning Algorithms to Estimate Soil Organic Carbon Variability with Environmental Variables and Soil Nutrient Indicators in an Alluvial Soil. *Land* **2020**, *9*, 487. [CrossRef]
64. Alasta, A. Using Remote Sensing Data to Identify Iron Deposits in Central Western Libya. In Proceedings of the International Conference on Emerging Trends in Computer and Image Processing (ICETCIP'2011), Bangkok, Thailand, 27–28 December 2011; pp. 56–61. Available online: https://www.researchgate.net/publication/325550303_Using_Remote_Sensing_data_to_identify_iron_deposits_in_central_western_Libya (accessed on 15 March 2025).
65. Dubčáková, R. Eureqa: Software Review. *Genet. Program. Evolvable Mach.* **2011**, *12*, 173–178. [CrossRef]
66. Amen, R.; Hameed, J.; Albashar, G.; Kamran, H.W.; Hassan Shah, M.U.; Zaman, M.K.U.; Mukhtar, A.; Saqib, S.; Ch, S.I.; Ibrahim, M.; et al. Modelling the Higher Heating Value of Municipal Solid Waste for Assessment of Waste-to-Energy Potential: A Sustainable Case Study. *J. Clean. Prod.* **2021**, *287*, 125575. [CrossRef]
67. Pérez, M.J.; Cuello, A.S.; Zampini, I.C.; Ordoñez, R.M.; Alberto, M.R.; Quispe, C.; Schmeda-Hirschmann, G.; Isla, M.I. Polyphenolic Compounds and Anthocyanin Content of Prosopis Nigra and Prosopis Alba Pods Flour and Their Antioxidant and Anti-Inflammatory Capacities. *Food Res. Int.* **2014**, *64*, 762–771. [CrossRef] [PubMed]
68. Zveushe, O.K.; de Dios, V.R.; Zhang, H.; Zeng, F.; Liu, S.; Shen, S.; Kang, Q.; Zhang, Y.; Huang, M.; Sarfaraz, A.; et al. Effects of Co-Inoculating *Saccharomyces* Spp. with Bradyrhizobium Japonicum on Atmospheric Nitrogen Fixation in Soybeans (*Glycine max* (L.)). *Plants* **2023**, *12*, 681. [CrossRef]
69. Díaz Lezcano, M.I.; Gamarra Lezcano, C.C.; Vera de Ortiz, M.L.; Santa Cruz Estigarribia, A.V.; Díaz Lezcano, M.I.; Gamarra Lezcano, C.C.; Vera de Ortiz, M.L.; Santa Cruz Estigarribia, A.V. Contenido de Nitrógeno En Suelos de Sistemas Silvopastoriles de Prosopis Spp. Del CHaco Central Paraguayo. *Rev. Cub. Cienc. For.* **2021**, *9*, 226–240.
70. Sadeq, M.A.M.; Abido, M.S.; Salih, A.A.; Alkhuzai, J.A. The Effects of Mesquite (*Prosopis juliflora*) on Soils and Plant Communities in the Deserted Rangelands of Bahrain. *Int. J. For. Res.* **2020**, *2020*, 8810765. [CrossRef]
71. Kong, W.; Liu, M.; Felker, P.; Ewens, M.; Bessega, C.; Pometti, C.; Wang, J.; Xu, P.; Teng, J.; Wang, J.; et al. Genome and Evolution of Griseb., a Drought and Salinity Tolerant Tree Legume Crop for Arid Climates. *Plants People Planet* **2023**, *5*, 933–947. [CrossRef]
72. Wu, L.; Qin, M.; Muneer, M.A.; Bao, J.; Chen, X.; Yang, Y.; Huang, J.; Zhang, S.; Su, D.; Yan, X. Soil pH and Organic Matter: Key Edaphic Factors in Sustaining Optimum Yield and Quality of Pomelo Fruit. *Sci. Hortic.* **2024**, *337*, 113524. [CrossRef]
73. Martins-Noguerol, R.; Matías, L.; Pérez-Ramos, I.M.; Moreira, X.; Francisco, M.; Pedroche, J.; DeAndrés-Gil, C.; Gutiérrez, E.; Salas, J.J.; Moreno-Pérez, A.J.; et al. Propiedades Fisicoquímicas Del Suelo Asociadas al Rendimiento y Composición Fitoquímica de La Halófita Comestible. *Crithmum Maritimum. Sci. Total Environ.* **2023**, *869*, 161806. [CrossRef]
74. Mao, Y.; Chai, X.; Zhong, M.; Zhang, L.; Zhao, P.; Kang, Y.; Guo, J.; Yang, X. Efectos de Los Nutrientes Nitrógeno y Magnesio Sobre El Crecimiento de La Planta, Calidad, Características Fotosintéticas, Metabolismo Antioxidante y Hormonas Endógenas de La Col Rizada China (*Brassica albograbra* Bailey). *Sci. Hortic.* **2022**, *303*, 111243. [CrossRef]
75. Jadeja, A.S.; Rajani, A.V.; Kaneriya, S.C.; Hirpara, D.V. Nutrient Content, Uptake, Quality of Chickpea (Cicer Arietinum L.) and Fertility Status of Soil as Influenced by Fertilization of Potassium and Sulphur. *Int. J. Curr. Microbiol. App. Sci.* **2019**, *8*, 2351–2355. [CrossRef]
76. Xing, Y.; Niu, X.; Wang, N.; Jiang, W.; Gao, Y.; Wang, X. The Correlation between Soil Nutrient and Potato Quality in Loess Plateau of China Based on PLSR. *Sustainability* **2020**, *12*, 1588. [CrossRef]
77. Taghavi, M.; Bakhshi, K.; Zarei, A.; Hoseinzadeh, E.; Gholizadeh, A. Soil Pollution Indices and Health Risk Assessment of Metal(Loid)s in the Agricultural Soil of Pistachio Orchards. *Sci. Rep.* **2024**, *14*, 8971. [CrossRef] [PubMed]

78. Vallejos-Torres, G.; Gaona-Jimenez, N.; Arevalo, A.A.; Paredes, C.; Lozano, A.; Saavedra-Ramírez, J.; Arévalo, L.A.; Reátegui, K.; Mendoza-Caballero, W.; Marín, C. Cadmium uptake and mycorrhization by cacao clones in agroforestry and monoculture systems of Peruvian Amazon. *Bioagro* **2023**, *35*, 237–246. [CrossRef]
79. Angon, P.B.; Islam, M.S.; Kc, S.; Das, A.; Anjum, N.; Poudel, A.; Suchi, S.A. Sources, Effects and Present Perspectives of Heavy Metals Contamination: Soil, Plants and Human Food Chain. *Heliyon* **2024**, *10*, e28357. [CrossRef] [PubMed]
80. Chen, Z.; Muhammad, I.; Zhang, Y.; Hu, W.; Lu, Q.; Wang, W.; Huang, B.; Hao, M. Transfer of Heavy Metals in Fruits and Vegetables Grown in Greenhouse Cultivation Systems and Their Health Risks in Northwest China. *Sci. Total Environ.* **2021**, *766*, 142663. [CrossRef]
81. Eid, E.M.; Shaltout, K.H.; Alamri, S.A.M.; Alrumman, S.A.; Hussain, A.A.; Sewelam, N.; El-Bebany, A.F.; Alfarhan, A.H.; Picó, Y.; Barcelo, D. Modelos de Predicción Basados En Las Propiedades Del Suelo Para Evaluar La Absorción de Ocho Metales Pesados Por Plantas de Tomate (*Lycopersicon Esculentum* Mill.) Cultivadas En Suelos Agrícolas Modificados Con Lodos de Depuradora. *J. Environ. Chem. Eng.* **2021**, *9*, 105977. [CrossRef]
82. Villalba, R.; Denis Ibars, J.; Martínez, K.; Coronel, E.; Friesen, A.; Mereles, L. Variations in the Composition of "Algarrobas" (*Prosopis* sp.) Flours Paraguayan Chaco. *Biol. Life Sci. Forum* **2022**, *17*, 25. [CrossRef]
83. Bigne, F.; Sciammaro, L.P.; Conforti, P.; Salinas, M.V.; Ferrero, C.; Puppo, M.C. Alimentos Con Harina de *Prosopis* spp.: Productos Horneados Comunes y Nuevos. In *Prosopis as a Heat Tolerant Nitrogen Fixing Desert Food Legume*; Puppo, M.C., Felker, P., Eds.; Academic Press: Cambridge, MA, USA, 2022; pp. 333–340. ISBN 978-0-12-823320-7.
84. Jhajharia, K.; Mathur, P. Prediction of Crop Yield Using Satellite Vegetation Indices Combined with Machine Learning Approaches. *Adv. Space Res.* **2023**, *72*, 3998–4007. [CrossRef]
85. Jeya Kumaran, V.; Mohidem, N.A.; Che'Ya, N.N.; Fazlil Ilahi, W.F.; Arif Shah, J.; Sahwee, Z.; Yusof, N.; Omar, M.H. How Can Aerial Imagery and Vegetation Indices Algorithms Monitor the Geotagged Crop? *Egypt. J. Remote Sens. Space Sci.* **2024**, *27*, 628–636. [CrossRef]
86. Hernandez, C.M.; Correndo, A.; Kyveryga, P.; Prestholt, A.; Ciampitti, I.A. On-Farm Soybean Seed Protein and Oil Prediction Using Satellite Data. *Comput. Electron. Agric.* **2023**, *212*, 108096. [CrossRef]
87. Hou, L.; Liu, Z.; Zhao, J.; Ma, P.; Xu, X. Comprehensive Assessment of Fertilization, Spatial Variability of Soil Chemical Properties, and Relationships among Nutrients, Apple Yield and Orchard Age: A Case Study in Luochuan County, China. *Ecol. Indic.* **2021**, *122*, 107285. [CrossRef]
88. Zahir, S.A.D.M.; Jamlos, M.F.; Omar, A.F.; Jamlos, M.A.; Mamat, R.; Muncan, J.; Tsenkova, R. Review—Plant Nutritional Status Analysis Employing the Visible and near-Infrared Spectroscopy Spectral Sensor. *Spectrochim. Acta A Mol. Biomol. Spectrosc.* **2024**, *304*, 123273. [CrossRef] [PubMed]
89. Du, M.; Noguchi, N.; Ito, A.; Shibuya, Y. Correlation Analysis of Vegetation Indices Based on Multi-Temporal Satellite Images and Unmanned Aerial Vehicle Images with Wheat Protein Contents. *Eng. Agric. Environ. Food* **2019**, *14*, 86–94. [CrossRef] [PubMed]
90. Savaşlı, E.; Karaduman, Y.; Önder, O.; Ateş, Ö. Prediction of Grain Protein Content and Gluten Quality of Bread Wheat in the Early Vegetation Period by Optical Sensors. *J. Cereal Sci.* **2021**, *102*, 103354. [CrossRef]
91. Savaşlı, E.; Önder, O.; Karaduman, Y.; Özen, D.; Dayıoğlu, R.; Özdemir, S.; Ateş, Ö.; Ekïz, M.; Erşahin, S. Developing Early-Estimating Normalized Difference Vegetation Index Calibrations for Grain Yield and Technological Quality of Bread Wheat in Semi-Arid Rainfed Conditions. *J. Cereal Sci.* **2024**, *120*, 104053. [CrossRef]
92. Fu, Z.; Yu, S.; Zhang, J.; Xi, H.; Gao, Y.; Lu, R.; Zheng, H.; Zhu, Y.; Cao, W.; Liu, X. Combining UAV Multispectral Imagery and Ecological Factors to Estimate Leaf Nitrogen and Grain Protein Content of Wheat. *Europ. J. Agron.* **2022**, *132*, 126405. [CrossRef]
93. Wang, L.; Tian, Y.; Yao, X.; Zhu, Y.; Cao, W. Predicting Grain Yield and Protein Content in Wheat by Fusing Multi-Sensor and Multi-Temporal Remote-Sensing Images. *Field Crops Res.* **2014**, *164*, 178–188. [CrossRef]
94. Pullanagari, R.R.; Yule, I.J.; Hedley, M.J.; Tuohy, M.P.; Dynes, R.A.; King, W.M. Multi-Spectral Radiometry to Estimate Pasture Quality Components. *Precis. Agric.* **2012**, *13*, 442–456. [CrossRef]
95. Arogoundade, A.M.; Mutanga, O.; Odindi, J.; Naicker, R. The Role of Remote Sensing in Tropical Grassland Nutrient Estimation: A Review. *Environ. Monit. Assess.* **2023**, *195*, 954. [CrossRef]
96. Tiwari, D.C.; Negi, P.; Thakur, S.; Rana, S.K.; Pandey, R.; Bhatt, I.D.; Nautiyal, S. Analyzing Climatic and Non-Climatic Impacts on Structure, Phenology and Functions of Western Himalayan Forests. *Ecol. Indic.* **2025**, *174*, 113511. [CrossRef]
97. Tasnim, N.; Hossain, M.R.; Fayeem, H.A.M.; Mostofa, Z.B.; Anika, T.T.; Mou, M.; Modabber, A.; Zaddary, A.M.; Gupta, A.D.; Marma, M.; et al. Towards Data-Driven Tropical Forest Restoration: Uncovering Spatial Variation, Interactions and Historical Management Effects on Nutrients along Soil Depth Gradients. *Sci. Total Environ.* **2024**, *954*, 176756. [CrossRef]